Astronomy & Astrophysics manuscript no.
(will be inserted by hand later)

Re-examining the X-Ray versus Spin-Down Luminosity Correlation of Rotation Powered Pulsars

Andrea Possenti[1], Rossella Cerutti[2], Monica Colpi[3], and Sandro Mereghetti[4]

[1] Osservatorio Astronomico di Bologna, via Ranzani 1, I-40127 Bologna, Italy
email: phd@tucanae.bo.astro.it
[2] Dipartimento di Fisica, Università di Milano , via Celoria 16, I-20133 Milano, Italy
e-mail: rossella@ifctr.mi.cnr.it
[3] Dipartimento di Fisica, Università di Milano Bicocca, Piazza della Scienza 3, I-20126 Milano, Italy
email: colpi@castore.mib.infn.it
[4] Istituto di Astrofisica Spaziale e Fisica Cosmica, Sezione di Milano "G.Occhialini", CNR, via Bassini 15, I-20133 Milano, Italy
email: sandro@ifctr.mi.cnr.it

Accepted for publication by *Astronomy & Astrophysics*

Abstract. The empirical relation between the X-ray luminosity (in the 2-10 keV band) and the rate of spin-down energy loss $L_{\rm sd}$ of a sample of 39 pulsars is re-examined considering recent data from *ASCA, RXTE, BeppoSAX, Chandra*, and *XMM-Newton* and including statistical and systematic errors. The data show a significant scatter around an average correlation between $L_{\rm x,(2-10)}$ and $L_{\rm sd}$. By fitting a dependence of $L_{\rm x,(2-10)}$ on the period P and period derivative $\dot{P}$ of the type $L_{\rm x,(2-10)} \propto P^a \dot{P}^b$, we obtain $a = -4.00$ and $b = +1.34$ (i.e. $a \simeq -3b$). This translates into the relation $L_{\rm x,(2-10)} = L_{\rm x,nor} \left(L_{\rm sd}/{\rm erg\ s^{-1}}\right)^{1.34}$ with a normalization $L_{\rm x,nor} = 10^{-15.3}$ erg s^{-1}. However, the reduced χ^2 is large ($= 7.2$) making the fit unacceptable on statistical ground. All the X-ray luminosities lie below a critical line $L_{\rm x,crit}$: the corresponding efficiency of conversion of rotational energy into 2-10 keV X-rays is $\eta_{\rm x} = (L_{\rm x,crit}/L_{\rm sd}) \propto L_{\rm sd}^{0.48}$ and varies, within the sample, between 0.1 and 80%. The large dispersion of $L_{\rm x}$ below $L_{\rm x,crit}$ indicates that other physical parameters uncorrelated with P and $\dot{P}$ need to be included to account for the observed emission at X-ray energies. We indicate a few possibilities that all conspire to reduce $L_{\rm x,(2-10)}$.

Key words. Radiation mechanisms: non-thermal – star: neutron – pulsar: general – X-rays: general – γ-ray: general

1. Introduction

About 40 of the nearly 1,400 known radio pulsars (Manchester 2001) have been so far detected in the X-ray range. Despite the great differences in their rotational parameters, magnetic field and age, these rotation-powered X-ray sources seem to obey a simple empirical law. The data reveal a correlation between their high-energy luminosity and their spin-down luminosity $L_{\rm sd} = 4\pi^2 I \dot{P}/P^3$, where P and $\dot{P}$ are the spin period and its derivative, and I is the neutron star momentum of inertia that we assume equal to 10^{45} g cm^2.

This correlation was first noticed in a small set of radio pulsars by Seward and Wang (1988), and later investigated by Becker and Trümper (1997; BT97 hereafter) using a sample of 27 powered pulsars detected with *ROSAT* in the soft energy band (0.1-2.4 keV). BT97 described the available data with a simple scaling relation

$$L_{\rm x} \simeq 10^{-3} L_{\rm sd} \quad . \tag{1}$$

However, a harder energy interval seems preferred to explore the nature of the X-ray emission resulting from the rotational energy loss: at energies above ∼2 keV the contribution from the neutron star cooling and the spectral fitting uncertainties due to interstellar absorption are reduced. Saito (1998) examined the correlation between $L_{\rm sd}$ and the pulsed X–ray luminosity using a sample of radio pulsars detected at high energies with *ASCA* (2-10 keV) finding the scaling relation

$$L_{\rm x,(2-10)} \simeq 10^{-21} L_{\rm sd}^{3/2} \quad . \tag{2}$$

None of these studies included the statistical and systematic uncertainties on $L_{\rm x}$ resulting from the errors on the X-ray fluxes and on the poorly known distances of

Send offprint requests to: A. Possenti

most pulsars. A proper treatment of these uncertainties is required to quantify the strength of the correlation.

The physical origin of the non-thermal X-ray emission from radio pulsars is uncertain. Polar cap models give predictions on the pulsed X-ray luminosity, which is attributed to inverse Compton scattering of higher order generation pairs on soft photons emitted by the surface of the neutron star and/or by hot polar caps (Zhang & Harding 2000). The soft tail in the inverse Compton scattering spectrum can explain the non-thermal X-ray component observed in many pulsars.

Outer gap models attribute the pulsed non-thermal X-ray emission to synchrotron radiation of downward cascades from the outer gap particles, and include (as in the inner gap models) a thermal component from the hot polar caps heated by impinging particles. Both models are consistent with the scaling relation $L_{\rm x} \propto L_{\rm sd}$ (Cheng, Gil, & Zhang 1998) in the *ROSAT* domain, but are in conflict with the observations in the *ASCA* (Zhang & Harding 2000) domain where they over or under-predict the values of $L_{\rm x}$ (relative to relation [2]). In polar cap models, these discrepancies can be accounted for by invoking *ad hoc* model parameters for the single sources, due to the difficulty in tracking the full cascade of particles and photons down to X-ray energies, coupled with the uncertainties in the temperature of the polar cap and of the whole surface.

The correlation between $L_{\rm x}$ and $L_{\rm sd}$ is even more difficult to quantify when considering that pulsed emission is observed only in 15 of the sources. Thus, for most of the pulsars, the total luminosity $L_{\rm x}$ can be considered only as an upper limit on the pulsed component. $L_{\rm x}$ often contains also the (unpulsed) contribution resulting from pulsar wind nebular emission (Chevalier 2000) which is in end related to the spin parameters P and $\dot{P}$.

For a comparison of the theoretical predictions with the observations, a statistical analysis of the data seems useful. Given the improved capabilities of the *Chandra* and *XMM-Newton* observatories, it is now timely to reconsider the correlation $L_{\rm x}$ versus $L_{\rm sd}$ in statistical terms, and this is the aim of our paper.

In §2 we describe the current sample and the criteria used to account for the uncertainties in $L_{\rm x}$. In §3 we present the results. In §4 we comment on the possible origin of the large scatter seen in the data and in §5 we summarize our conclusions.

2. Criteria for the data analysis

Our aim is to estimate the fraction of the rotational energy loss of a neutron star going into X-rays. This excludes from the sample the X-ray pulsars powered by accretion from binary companions (see e.g. Bildsten et al. 1997), and the Anomalous X-ray Pulsars (Mereghetti 2002), the luminosities of which are inconsistent with rotational energy loss in case of neutron stars. According to these criteria, the current sample consists of the 41 pulsars listed in Table 1.

Even in the case of spin-down powered neutron stars, some contribution(s) to the X-ray flux can derive from cooling. Thus we include only the following components in the calculation of the X-ray luminosity: *(i)* the non-thermal (pulsed) emission that originates in the neutron star magnetosphere; *(ii)* the thermal emission resulting from the re-heating of (parts of) the neutron star surface by backward accelerated particles; *(iii)* the flux from the extended synchrotron nebulae powered by the relativistic particles and/or magnetic fields ejected by the neutron star. As a rule, when possible we subtracted the contribution to the X-ray emission from the extended supernova shells. At energies $\gtrsim 2$ keV, the contribution from the neutron star cooling becomes unimportant. Thus, by considering the energy range 2-10 keV we reduce the uncertainties related to the subtraction of the cooling components.

We reviewed all the data in the literature for each source of our sample. When good observations were available in the 2-10 keV band, we adopted the reported flux. When only fluxes in a different energy range were available, we converted them to our range, adopting the parameters of the best spectral fit reported in the literature (see the references in Table 1). The luminosities $L_{\rm x,(2-10)}$ are calculated assuming isotropic emission and the distances listed in Table 1.

As a main improvement with respect to previous similar studies, we derive a *weighted fit* of the $L_{\rm x}$ versus $L_{\rm sd}$ data. For this purpose, we have taken into account the uncertainty associated to each value of $L_{\rm x}$. Contributions to such uncertainties have different origins:

(a) **Uncertainties in the distances**; for most of the pulsars, we have used the distances derived from the dispersion measure (DM; Pulsar Catalogue `http://pulsar.princeton.edu/pulsar/catalog`). They rely on a model for the electron distribution of the interstellar medium (Taylor & Cordes 1993). For individual sources this can lead to an error in the distance up to a factor $\gtrsim 3$ (e.g. the case of PSR J1119−6127, Camilo et al. 2000, Crawford et al. 2001), but, when averaged over the pulsar population, the typical errors reduce significantly (Taylor & Cordes 1993). When only the distance inferred from the DM was available, we conservatively adopted an uncertainty of ±40%. This translates in an error ~ 0.3 in $\log L_{\rm x}$. When other determinations of d exist (e.g. from parallax measurements or from associations with supernova remnants) we opted for the most accurate ones, assuming the uncertainties reported for the related measure.

(b) **Statistical errors in the number of photons**; the errors due to photon counting statistics dominate the weak pulsars first detected with *ROSAT*, yielding uncertainties up to ~ 0.5 in $\log L_{\rm x}$; statistical errors in the count rate are negligible for brighter objects.

(c) **Errors depending on interstellar absorption**; the conversion from the observed flux to that emitted at the source depends on the amount of interstellar ab-

Table 1. Parameters and emission of the 41 sample pulsars

Pulsar PSR	P ms	$\dot{P}$ 10^{-15} s s^{-1}	N_H 10^{21} cm^{-2}	*distance* kpc	α or kT keV	*Obs Band* keV	*Detector*	$f^{(2-10)}$ erg s^{-1}cm^{-2}	$\log L_X^{(2-10)}$ erg s^{-1}	ref
J0030+0451	4.87	$1.00 \cdot 10^{-5}$	2.15 ± 0.85	0.230 ± 0.092	2 ± 0.2	0.1–2.4	PSPC	$(1.27^{+0.95}_{-0.61}) \cdot 10^{-13}$	$29.88^{+0.54}_{-0.73}$	1
J0218+4232	2.32	$7.50 \cdot 10^{-5}$	2 ± 2	5.70 ± 2.28	0.94 ± 0.22	2.0–10.0	MECS	$(4.30^{+0.28}_{-0.22}) \cdot 10^{-13}$	$33.20^{+0.32}_{-0.47}$	2
J0437–4715	5.76	$1.86 \cdot 10^{-5}$	$0.8^{+1}_{-0.6}$	0.178 ± 0.026	2.35 ± 0.35	0.1–2.4	HRI	$(4.30^{+1}_{-1}) \cdot 10^{-13}$	$30.19^{+0.21}_{-0.25}$	3,4
J0751+1807	3.48	$8.00 \cdot 10^{-6}$	$4.4^{+4.6}_{-0.4}$	2 ± 0.8	2 ± 0.2	0.1–2.4	PSPC	$(4.29^{+3.54}_{-1.44}) \cdot 10^{-14}$	$31.29^{+0.55}_{-0.62}$	3
J1012+5307	5.26	$1.46 \cdot 10^{-5}$	0.06 ± 0.01	0.520 ± 0.208	2.3 ± 0.2	0.1–2.4	PSPC	$(1.25^{+0.89}_{-0.61}) \cdot 10^{-14}$	$29.58^{+0.53}_{-0.73}$	3
J1024–0719	5.16	$2.99 \cdot 10^{-6}$	0.2 ± 0.05	0.350 ± 0.140	2 ± 0.2	0.1–2.4	HRI	$(8.86^{+4.70}_{-3.36}) \cdot 10^{-15}$	$29.09^{+0.50}_{-0.79}$	3
J1744–1134	4.07	$7.13 \cdot 10^{-6}$	0.1 ± 0.05	$0.357^{+0.043}_{-0.035}$	2 ± 0.2	0.1–2.4	HRI	$(6.44^{+4.08}_{-2.86}) \cdot 10^{-15}$	$28.97^{+0.32}_{-0.40}$	3
B1821–24	3.05	$1.62 \cdot 10^{-3}$	2.9 ± 2.3	5.1 ± 0.5	1.89 ± 0.21	0.7–10.0	GIS	$(1.25^{+0.33}_{-0.69}) \cdot 10^{-12}$	$33.56^{+0.18}_{-0.44}$	5
B1937+21	1.56	$1.06 \cdot 10^{-4}$	21 ± 5	3.60 ± 1.44	$1.71^{+0.05}_{-0.08}$	0.5–10.0	LECS+MECS	$(3.70^{+0.40}_{-0.40}) \cdot 10^{-13}$	$32.73^{+0.39}_{-0.55}$	6
J2124–3358	4.93	$1.30 \cdot 10^{-5}$	0.35 ± 0.15	0.25 ± 0.10	2 ± 0.2	0.1–2.4	HRI	$(8.26^{+0.45}_{-3.48}) \cdot 10^{-14}$	$29.77^{+0.32}_{-0.68}$	7
B0950+08	253.07	0.229		0.127 ± 0.013		0.1–2.4	PSPC	$(2.3^{+0.7}_{-0.7}) \cdot 10^{-14}$	$28.62^{+0.42}_{-0.62}$	3
B1929+10	226.52	1.16	0.1 ± 0.05	0.25 ± 0.08	0.44 ± 0.046 [c]	0.5–5.0	SIS	$(5.6^{+1.5}_{-1.4}) \cdot 10^{-14}$	$29.60^{+0.34}_{-0.46}$	8
B0823+26	530.66	1.71		0.380 ± 0.152		0.1–2.4	PSPC	$(0.6^{+0.2}_{-0.2}) \cdot 10^{-14}$	$28.99^{+0.42}_{-0.62}$	3
B0114+58	101.44	5.85	2.57 ± 0.2	2.14 ± 0.856	2.1 ± 0.2	0.1–2.4	PSPC	$(4.25^{+4.25}_{-0.??}) \cdot 10^{-15}$	$30.34^{+0.59}_{-0.??}$	9
B0355+54	156.38	4.40	0.2 ± 0.2	2.10 ± 0.84	2 ± 0.5	0.1–2.4	PSPC	$(1.16^{+3.04}_{-0.94}) \cdot 10^{-13}$	$31.76^{+0.85}_{-1.17}$	10
J0538+2817	143.16	3.67	0.6 ± 0.6	1.5 ± 0.6	1.5 ± 0.5	0.1–2.4	PSPC	$(8.00^{+8.00}_{-0.??}) \cdot 10^{-16}$	$29.31^{+0.59}_{-0.??}$	11
B0633+17	237.09	11.0	0.13 ± 0.13	$0.154^{+0.059}_{-0.034}$	2.19 ± 0.35	0.7–5.0	GIS	$(7.94^{+3.0}_{-2.2}) \cdot 10^{-14}$	$29.33^{+0.42}_{-0.36}$	12
B0656+14	384.89	55.0	0.17 ± 0.17	$0.28^{+0.20}_{-0.10}$	1.5 ± 1.1	1.0–5.0	SIS	$(2.05^{+1.72}_{-0.74}) \cdot 10^{-13}$	$30.26^{+0.73}_{-0.58}$	13
B1055–52	197.11	5.83	0.26 ± 0.06	0.5 ± 0.2	1.5 ± 0.3	2.0–10.0	GIS	$(1.06^{+0.10}_{-0.09}) \cdot 10^{-14}$	$29.48^{+0.33}_{-0.48}$	14
B1951+32	39.53	5.84	3.4 ± 0.5	2.5 ± 0.2	2.1 ± 0.3	0.1–2.4	PSPC	$(2.04^{+0.85}_{-0.79}) \cdot 10^{-12}$	$33.16^{+0.22}_{-0.28}$	15
B0833–45	89.33	$1.25 \cdot 10^2$	0.4 ± 0.1	0.25 ± 0.03	2.2 ± 0.4	0.2–8.0	ACIS-S	$(1.03^{+1.04}_{-0.55}) \cdot 10^{-11}$	$31.86^{+0.40}_{-0.44}$	16
B1046–58	123.67	96.3	5 ± 1	2.98 ± 1.19	2 ± 0.2	0.4–10.0	SIS	$(2.50^{+0.66}_{-0.58}) \cdot 10^{-13}$	$32.40^{+0.39}_{-0.56}$	17
J1105–6107	63.19	15.8	8.55 ± 5.25	7.0 ± 2.8	1.8 ± 0.4	2.0–10.0	GIS	$(6.47^{+1.18}_{-1.04}) \cdot 10^{-13}$	$33.55^{+0.37}_{-0.52}$	18
J1420–6048	68.18	83.2	22 ± 7	2.0 ± 0.8	1.6 ± 0.4 [b]	2.0–10.0	GIS	$(4.70^{+0.77}_{-0.74}) \cdot 10^{-12}$	$33.33^{+0.36}_{-0.52}$	19
B1706–44	102.46	93.0	3.45 ± 3.45	1.80 ± 0.72	1.9 ± 0.9	2.0–10.0	SIS+GIS	$(1.03^{+0.38}_{-0.24}) \cdot 10^{-12}$	$32.58^{+0.43}_{-0.56}$	20
B1757–24	124.90	$1.28 \cdot 10^2$	35 ± 12	$5.0^{+2.0}_{-0.7}$	1.6 ± 0.6	2.0–10.0	ACIS-S	$(7.9^{+0.6}_{-0.6}) \cdot 10^{-13}$	$33.37^{+0.20}_{-0.10}$	21
B1800–21	133.63	$1.34 \cdot 10^2$	13 ± 1	5.30 ± 2.12	2 ± 0.2	0.1–2.4	PSPC	$(1.78^{+0.70}_{-0.59}) \cdot 10^{-13}$	$32.75^{+0.45}_{-0.70}$	22
J1811–1926	64.67	44.0	13.8 ± 0.8	7.8 ± 2.5	1.89 ± 0.25	4.0–10.0	MECS	$(1.23^{+0.07}_{-0.11}) \cdot 10^{-11}$	$34.93^{+0.27}_{-0.38}$	23
B1823–13	101.45	75.5	40 ± 25	4.12 ± 1.65	2 ± 0.2	0.5–2.4	PSPC	$(1.70^{+4.4}_{-1.4}) \cdot 10^{-11}$	$34.51^{+0.85}_{-1.20}$	24
B1853+01	267.40	$2.08 \cdot 10^2$	2.57 ± 0.2	3.2 ± 1.3	2.3 ± 1.1	0.4–2.0	GIS	$(1.2^{+0.3}_{-0.3}) \cdot 10^{-12}$	$33.14^{+0.39}_{-0.57}$	25
J2229+6114	51.62	78.0	6.3 ± 1.3	3 ± 1	1.51 ± 0.14	2.0–10.0	ACIS-I	$(1.30^{+0.09}_{-0.08}) \cdot 10^{-12}$	$33.12^{+0.28}_{-0.38}$	26
B2334+61	495.28	$1.92 \cdot 10^2$	2 ± 1	2.5 ± 1	2 ± 0.2	0.1–2.4	PSPC	$(4.05^{+2.6}_{-1.7}) \cdot 10^{-14}$	$31.46^{+0.52}_{-0.86}$	27
J0205+6449	65.68	$1.93 \cdot 10^2$	3 ± 2	2.6 ± 0.6	1.9 ± 0.2 [b]	0.8–10.0	HRC	$(1.5^{+0.3}_{-0.3}) \cdot 10^{-11}$	$34.08^{+0.14}_{-0.21}$	28
B0531+21	33.52	$4.21 \cdot 10^2$	3 ± 0.5	2 ± 0.5	2.108 ± 0.006	0.3–10.0	MOS	$(9.93^{+0.09}_{-0.43}) \cdot 10^{-9}$	$36.65^{+0.20}_{-0.27}$	29
J0537–6910	16.11	51.0	6.9 ± 3.3	47.3 ± 0.8	$\frac{1.6 \pm 0.2}{2.55 \pm 0.15}$ [a] [b]	0.2–10.0	GIS	$(5.13^{+1.38}_{-1.37}) \cdot 10^{-12}$	$36.11^{+0.12}_{-0.15}$	30
B0540–69	50.53	$4.73 \cdot 10^2$	4.6 ± 4.6	47.3 ± 0.8	$\frac{1.83 \pm 0.13}{2.06 \pm 0.2}$ [a] [b]	0.2–10.0	ACIS-I	$(3.33^{+0.97}_{-1.29}) \cdot 10^{-11}$	$36.93^{+0.13}_{-0.23}$	31
J1119–6127	407.75	$4.02 \cdot 10^3$	15 ± 15	5 ± 3	$1.4^{+1.0}_{-1.2}$	0.7–5.0	GIS	$(4.74^{+6.8}_{-2.7}) \cdot 10^{-13}$	$33.13^{+0.80}_{-1.16}$	32
J1124–5916	135.31	$7.45 \cdot 10^2$	3.17 ± 0.15	4.8 ± 1.6	1.9 ± 0.2	2.0–8.0	ACIS-S	$(1.1^{+0.2}_{-0.2}) \cdot 10^{-11}$	$34.48^{+0.18}_{-0.31}$	33,34
B1509–58	150.66	$1.54 \cdot 10^3$	12.7 ± 12.7	4.2 ± 0.5	$\frac{1.358 \pm 0.014}{2.2 \pm 0.005}$ [a] [b]	2.0–250	PCA	$(1.05^{+0.06}_{-0.33}) \cdot 10^{-10}$	$35.32^{+0.12}_{-0.27}$	35
J1617–5055	69.36	$1.37 \cdot 10^2$	6.8 ± 6.8	4.5 ± 0.9	1.6 ± 0.3	3.5–10.0	GIS	$(8.86^{+0.49}_{-0.34}) \cdot 10^{-12}$	$34.31^{+0.18}_{-0.21}$	36
J1846–0258	323.60	$7.10 \cdot 10^3$	47 ± 8	19 ± 5	2.2 ± 0.1	3.0–20.0	PCA	$(3.90^{+0.4}_{-0.4}) \cdot 10^{-11}$	$36.22^{+0.28}_{-0.32}$	37,38

Refs: Note: [a] Pulsed component photon index; [b] compact nebula photon index; [c] polar cap black body temperature. Detector: PSPC and HRI are instruments aboard of *ROSAT*; GIS and SIS are intruments aboard of *ASCA*; LECS, MECS and PCA are instruments aboard of *Beppo-SAX*; ACIS-I, ACIS-S and HRC are instruments aboard of *Chandra*; MOS is an instrument aboard of *Newton-XMM*. Obs Band: is the energy band of the observation from which the fluxes reported in column 9 are measured or extrapolated. References: [1] Becker et al. 2000; [2] Mineo et al. 2000; [3] BT99; [4] Kawai et al. 1998; [5] Saito et al. 1997; [6] Nicastro et al. 2002; [7] Sakurai et al. 2001; [8] Wang, Halpern 1997; [9] Slane 1995; [10] Slane 1994; [11] Sun et al. 1995; [12] Halpern, Wang 1997; [13] Greiveldinger et al. 1996; [14] Cheng, Zhang 1999; [15] Chang, Ho 1997; [16] Pavlov et al. 2001; [17] Pivovaroff et al. 2000; [18] Gotthelf, Kaspi 1998; [19] Roberts et al. 2001; [20] Finley et al. 1998; [21] Kaspi et al. 2001; [22] Finley, Ogelman 1994; [23] Torii et al. 1999; [24] Finley et al. 1996; [25] Harrus et al. 1996; [26] Halpern et al. 2001; [27] BT97; [28] Murray et al. 2002; [29] Willingale et al. 2001; [30] Marshall, Gotthelf et al. 1998; [31] Kaaret et al. 2000; [32] Pivovaroff et al. 2001; [33] Hughes et al. 2001; [34] Camilo et al. 2002; [35] Marsden et al. 1997; [36] Torii et al. 1998; [37] Gotthelf et al. 2000; [38] Mereghetti et al. 2002

sorption, which is typically deduced (in a model dependent way) from the X-ray spectral fits. We evaluated the errors deriving from the poor knowledge of N_H on a case by case basis.

(d) **Errors depending on spectral and spatial modeling**; collecting area, integration time, spectral and spatial resolution span a large range of values for the observations of different sources, implying that they have been studied with different degree of details. This introduces strong differences in the uncertainties related to the modeling of each source. So we have studied them individually.

In the computation of the error bars we first varied $N_{\rm H}$ and the spectral parameters within the uncertainties reported in Table 1, taking the resulting maximum and minimum fluxes. The errors on $f_{\rm X}$ are then propagated

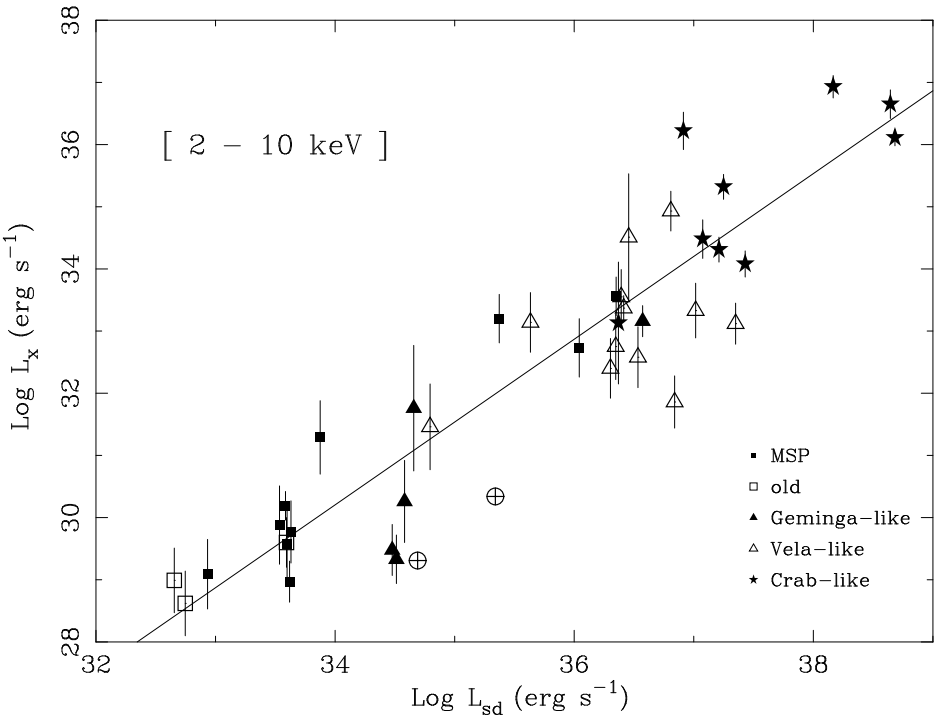

Fig. 1. The X-ray luminosity in the band (2-10) keV against the spin-down luminosity for the 41 sources of our sample. The objects are grouped in 5 classes and labeled accordingly: Millisecond Pulsar (*filled squares*), old pulsar (*empty squares*), Geminga-like (*filled triangles*), Vela-like (*empty triangles*) and Crab-like (*filled stars*). The *solid line* represents our equation [3]; it has been calculated on 39 objects (thus excluding PSR J0114+58 and PSR J0538+2817, also labeled with a circle filled with a cross and without their huge error bar; see Table 1).

accounting for the distance uncertainties and for the error due to photon counting statistics.

3. The current sample

The 41 pulsars listed in Table 1 can be naturally grouped into five classes, based on their intrinsic and observational characteristics.

I *Millisecond Pulsars* (*MSPs*): Six among the ten MSPs in our sample have been detected only by *ROSAT*, and four of these with a very low photon counting statistics (< 50 photons). This does not allow to asses which is their best spectral model. The objects studied in more detail with *ROSAT* indicate that non-thermal fits are preferred (Becker & Trümper 1999). However, recent observations with *Chandra* of the MSP population in the globular cluster 47 Tucanae (Grindlay et al. 2001), indicate that a thermal component may be present at energies $\lesssim 1.5$ keV. Considering that the possible thermal component would contribute only slightly to the luminosity in our energy range (2-10 keV), we have adopted for all the MSPs a power law spectrum with photon index $\alpha_{ph} = 2$ (so that the specific energy flux $f_\nu \propto \nu^{(-\alpha+1)}$). The list of sources belonging to this group is reported in the upper section of Table 1.

II *Old Pulsars:* Only three of the non recycled pulsars in our sample have characteristics ages ($\tau = P/2\dot{P}$) greater than 10^6 yr: PSR B0823+26, PSR B0950+08 and PSR B1929+10. *ASCA* observations of the latter two sources were reported by Wang & Halpern (1997), but it was later found that the results for PSR B0950+08 were affected by the presence of a nearby AGN (see note in Wang et al. 1998). The spectrum of PSR B1929+10 in the *ASCA* band can be described by thermal emission from a small fraction of the star surface ($\lesssim 10 - 30$ m in size). This is generally interpreted in terms of re-heating of the polar caps by backward accelerated particles in the magnetosphere. Assuming that the same interpretation is valid for PSR B0823+26 and PSR B0950+08, we use for these objects the flux obtained by scaling their ROSAT count rates to that of PSR B1929+10 and adopting large error bars.

III *Geminga-like:* This class contains the middle aged pulsars ($\tau \sim 10^5$ yr) for which the internal cooling gives a substantial contribution, at least at energies below $\sim$2 keV. For the three brightest objects of this group (Geminga, PSR B0656+14 and PSR B1055−52) accurate spectral modeling exist, allowing to estimate with a good accuracy and subtract the contribution from the cooling to $L_{\rm x}$. For PSR B1951+32 our adopted $L_{\rm x}$ derives mainly from the synchrotron nebula surrounding the pulsar. The remaining two sources (PSR B0114+58, PSR J0538+2817) are considerably weak preventing a detailed spectral analysis; therefore these two sources are not included in the statistical fit. However, in order to include them in the graphical representations of Figures 1 and 4, we have assumed a power-law model, with α as given in Table 1, and a ratio $\sim 10^{-3}$ between the flux in the power-law and the cooling component, i.e., an average between Geminga and PSR B1055−52. This could largely underestimate the flux if it is entirely of magnetospheric origin.

IV *Vela-like:* This is a rather inhomogeneous group of $\sim 10^4 - 10^5$ years old pulsars. Some of them are associ-

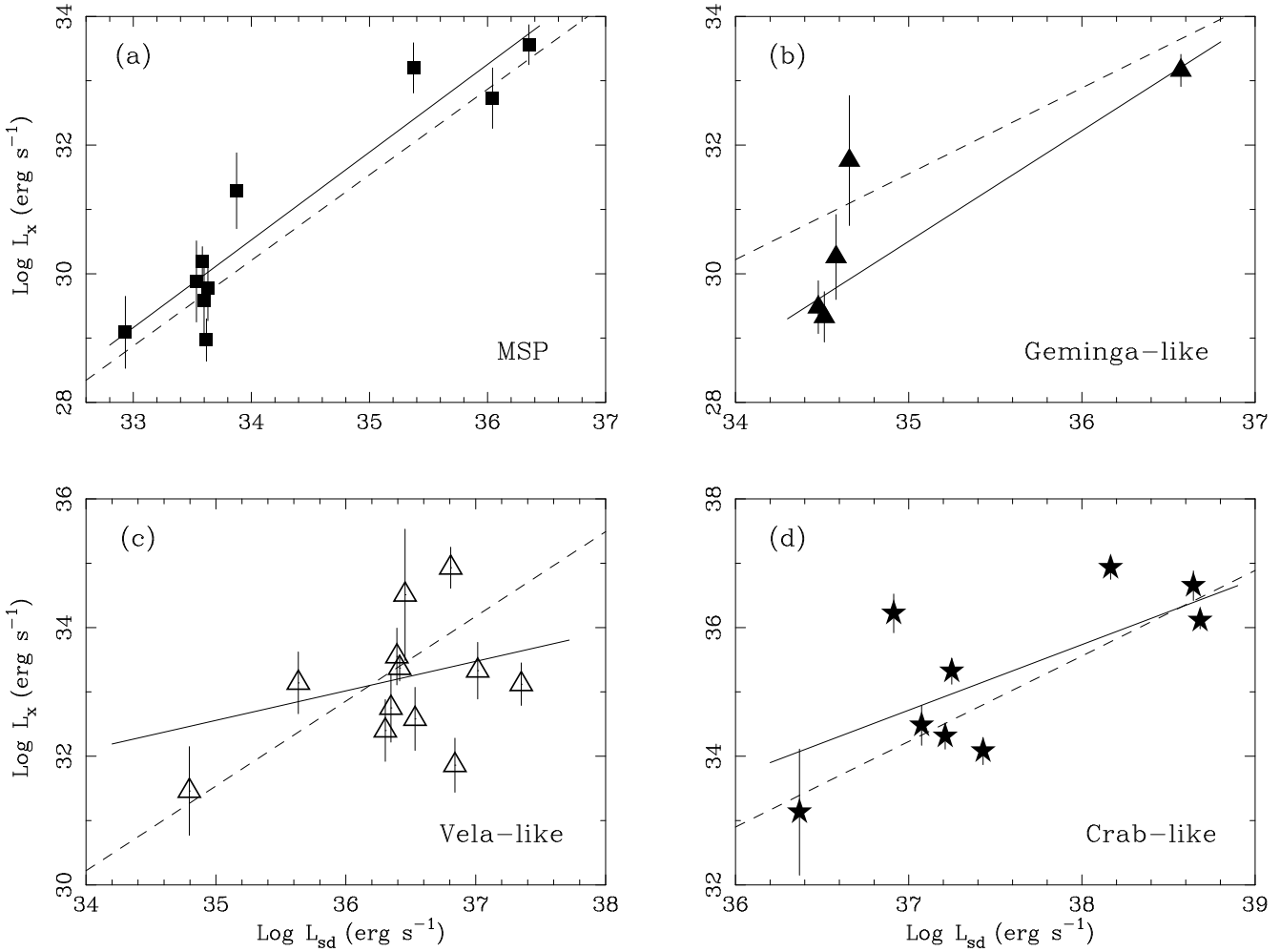

Fig. 2. The X-ray luminosity in the (2-10) keV band plotted against the spin-down luminosity for 4 subclasses of objects in our sample. The *solid lines* represent the best fits of a relation of the type $\log L_{\rm x,(2-10)} = m \log L_{\rm sd} - q$ calculated for the sources of each subclass: they are $\log L_{\rm x,(2-10)} = (1.38 \pm 0.10) \log L_{\rm sd} - 16.36 \pm 3.64$ for the Millisecond Pulsars (*panel a*), $\log L_{\rm x,(2-10)} = (1.71 \pm 0.17) \log L_{\rm sd} - 29.35 \pm 6.15$ for the Geminga-like sources (*panel b*), $\log L_{\rm x,(2-10)} = (0.46 \pm 0.23) \log L_{\rm sd} + 16.61 \pm 8.33$ for the Vela-like sources (*panel c*) and $\log L_{\rm x,(2-10)} = (1.02 \pm 0.10) \log L_{\rm sd} - 3.14 \pm 3.86$ for the Crab-like sources (*panel d*). The *dashed line* is the fit given in equation [3]: see text for details.

ated to supernova remnants. For most of these objects, the main contribution to $L_{\rm x,(2-10)}$ arises from their synchrotron nebulae, that typically have power-law spectra with α_{ph} in the range 1.5−2.3 (PSR B0833−45, PSR B1046−58, PSR J1105−6107, PSR B1706−44, PSR J1811−1926, PSR B1823−13, PSR B1853+01, PSR J2229+61). In the case of PSR B1757−24 the bulk of the emission in the (2–10 keV) band seems of magnetospheric origin, whereas in the cases of PSR J1420−6048, PSR B1800−21, PSR B2334+61 the number of collected photons is too small for a detailed analysis.

V *Crab-like:* These are the youngest pulsars in our sample. They have been directly seen in the hard energy band, and are usually bright enough for a careful examination of their spectra. Their emission consists of two components, a pulsed one of magnetospheric origin, and a second one (unpulsed) from the synchrotron nebula. The pulsars of this class are listed in the lower section of Table 1. Only for PSR J1119−6127 and PSR J1124−5916 observation prevents the possibility of disentangling the pulsed from the unpulsed components: for the former source due to the low photon statistics of the *ASCA* detection, for the latter object due to the poor time resolution of the adopted *Chandra* detector.

4. Results

To facilitate the comparison with previous works, we have first fitted 39 points in Figure 1 with a linear relation, obtaining

$$\log L_{\rm x,(2-10)} = 1.34 \log L_{\rm sd} - 15.34 \quad (3)$$

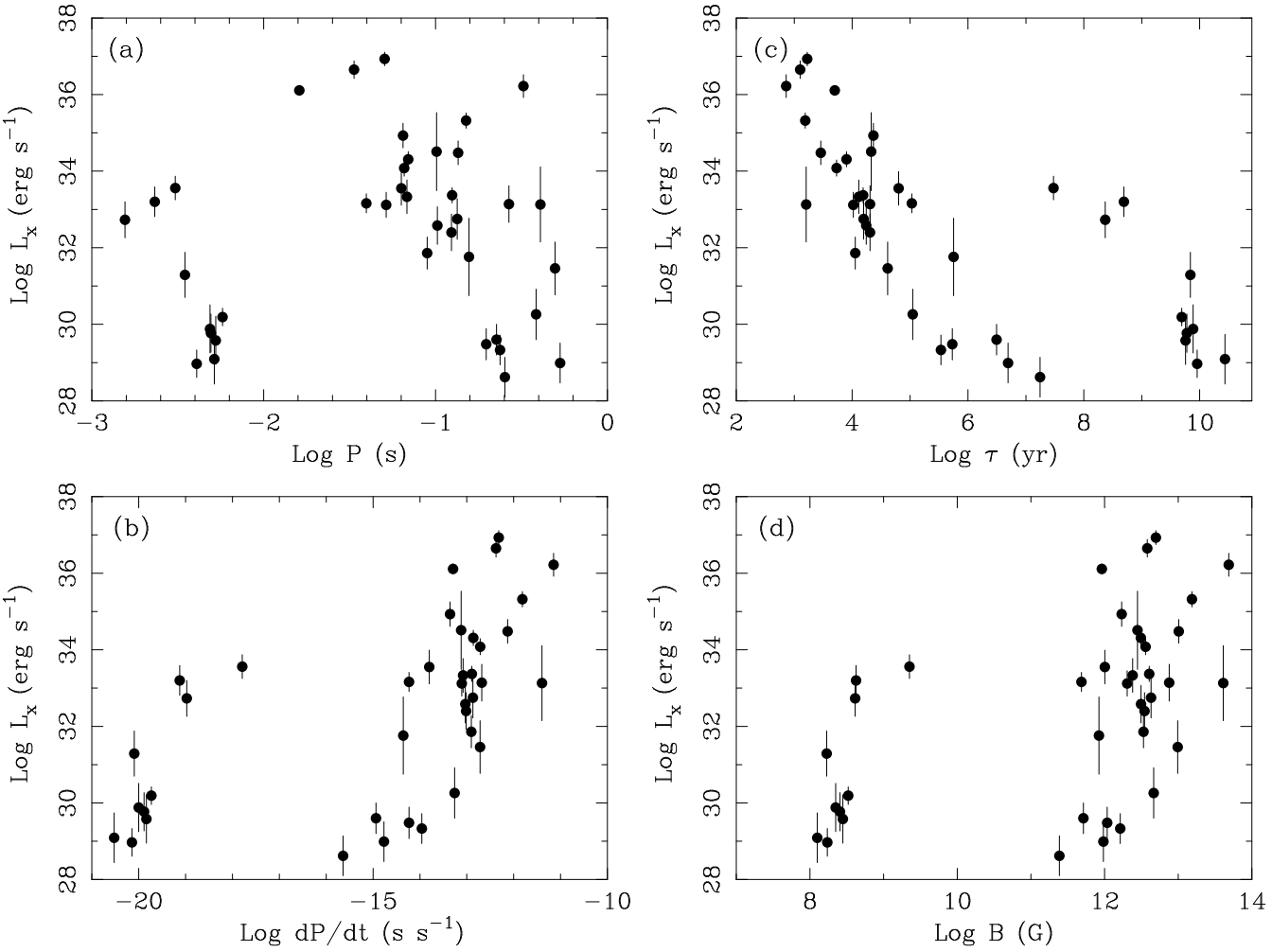

Fig. 3. X-ray luminosities in the (2-10) keV band plotted versus the rotational period (*panel a*), the period derivative (*panel b*), the characteristic age (*panel c*), and the surface magnetic field (*panel d*).

with a $\chi^2 = 259.4$ (solid line in Figure 1). The formal 1σ intervals of uncertainty are 1.34 ± 0.03 (for the slope) and 14.36 ± 1.11 (for the constant term). Thus the slope m of the relation (3) is slightly flatter than the value of 1.5 derived in the same energy interval for a sample of 15 objects by Saito (1998), who considered only the pulsed emission. At lower energies, *ROSAT* data instead suggest a slope of $m_{(0.1-2.4)} = 1.04 \pm 0.09$ for 27 sources (BT97), though a steeper dependence $m_{(0.1-2.4)} = 1.35$ was derived by Ögelman (1995) using a sample of 7 sources. At the intermediate energy range 0.2−4 keV Seward & Wang (1988) found a value of 1.39 based on a small sample of 8 pulsars. We note however that the empirical relation of $L_{\rm x}$ with $L_{\rm sd}$ is not fully satisfied as the fit of equation (3) is statistically unacceptable having an extremely large value of the reduced $\chi^2 \sim 7.0$. The scatter around this relation is remarkable, even when splitting the data in the different classes of sources, as shown in Figure 2.

In the caption of Figure 2, we have reported the results of the linear fit for 4 distinct subclasses of objects in our sample. We note that the Crab-like sources (panel d) are evenly distributed on both sides of the best-fit line of equation (3) (dashed line in all the panels of Figure 2), but their local best fit line (with a slope of $m_{\rm crab} = 1.02$) is flatter than that derived from fitting all data in our sample. Remarkably, the two sources located in the Magellanic Clouds (whose relative X-ray luminosity is not affected by uncertainties in the distance) even show an anticorrelation between $L_{\rm sd}$ and $L_{\rm x,(2-10)}$: PSR J0537−69 (whose $L_{\rm sd}$ is about 3 times greater than that of PSR B0540−69) appears about ten times dimmer in the *ASCA* band than PSR B0540−69: we note that the ratio between the two luminosities, for these two objects, scales with the ratio of their period derivatives $\dot{P}$.

Geminga and the other cooling pulsars have a relatively steep slope $m_{\rm gem} = 1.71$ and (with the exception of PSR B0355+54) are underluminous of $1 - 1.5$ dex relative to the dashed line (eq. [3]) describing the whole sample. This could suggest that either the (subtracted) thermal component has been overestimated or that these sources are preferred targets for the mechanisms which could reduce the luminosity in the 2-10 keV band (see §5).

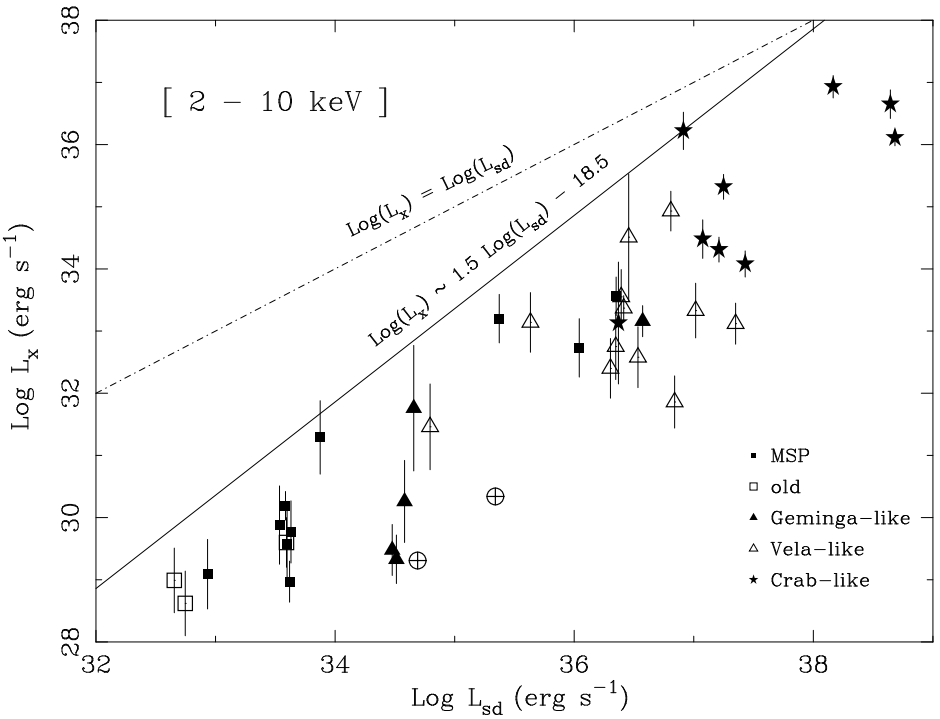

Fig. 4. The X-ray luminosity in the band (2-10) keV against the spin-down luminosity for the 41 sources of our sample. Objects and labels are as in Figure 1. The *dot-dashed line* represents the line $\log L_{\rm x,(2-10)} = \log L_{\rm sd}$, whereas the *solid line* is the critical line of equation [6], obtained excluding the two pulsars PSR J0114+58 and PSR J0538+2817. All points in this diagram locate below the solid line.

The typical spin down ages, the morphologies and the spectral characteristics of the Vela-like pulsars classify them between the Crab-like and the Geminga-like objects. Thus, it is not surprising that the data plotted for this group of sources (panel c of Figure 2) display features of both the Crab-like and the Geminga-like plots. In fact the slope $m_{\rm vela} = 0.46$ is much flatter than that of the entire sample and a significant number of these objects appear much dimmer than predicted by equation 3.

Finally, Figure 2 shows that the MSPs are the sources which better follow the general $\log L_{\rm x,(2-10)}$ vs $\log L_{\rm sd}$ relation, both in terms of slope $m_{\rm msp} = 1.38$ and of luminosities. Interestingly, the MSPs in 47 Tuc observed in the (0.5-2.5) keV interval with *Chandra* appear to have a weaker dependence of $L_{\rm x}$ on $L_{\rm sd}$ than those in the field, with a best median estimate for the slope of 0.55 ± 0.2 (Grindlay et al. 2002).

Figures 3a and 3b illustrate that the scatter in the values of $L_{\rm x,(2-10)}$ (already appearing in Figure 1) is even larger when the X-ray luminosities are plotted separately versus the periods and period derivatives. We also note the lack of any correlation between the plotted quantities. There are two physical ways of combining P and $\dot{P}$ to give the characteristic age ($\tau = P/2\dot{P}$) and the surface magnetic field ($B_s = 3.2 \times 10^{19}\sqrt{P\dot{P}}$ G) of a pulsar. In Figures 3c and 3d we report $L_{\rm x,(2-10)}$ versus these two quantities: while the spread in the data remains large, a correlation (already noted by BT97) is visible in $L_{\rm x,(2-10)}$ versus τ, when the subsample of the MSPs is excluded.

This suggests the possibility to improve the quality of the fit by using a more general function of P and $\dot{P}$. In fact, the proposed physical models for the X-ray emission rely on mechanisms depending on different combinations of these two quantities. Therefore, we have explored a fit of the type

$$\log L_{\rm x,(2-10)} \;=\; a \log P + b \log \dot{P} + c \; . \qquad (4)$$

Using a χ^2 minimization code, we found $a = -4.00 \pm 0.13$, $b = 1.34 \pm 0.03$, $c = 47.11 \pm 0.32$ with a $\chi^2 = 259.3$, implying that the fit is still unacceptable. Only enlarging the error bars on $\log L_{\rm x,(2-10)}$ up to absolutely unreliable values of ~ 0.9 (in units of log(erg s^{-1})), this modeling of the data would become statistically acceptable (with χ^2/d.o.f. $= 1.1$). Rearranging the best-fit, we get $\log L_{\rm x,(2-10)} = 1.34(-2.99 \log P + \log \dot{P} + c') = 1.34(-3 \log P + \log \dot{P} + c') + 0.02 \log P$. Since $\log P$ spans the interval $-3 \rightarrow 1$, the last addendum is of the order of the 1σ uncertainty on the constant term, and thus we can approximate the formula, getting

$$\log L_{\rm x,(2-10)} \;=\; 1.34 \log L_{\rm sd} \;-\; 15.30 \qquad (5)$$

which is very close to the best fit of equation (3). This exercise has shown that, when properly accounting for the uncertainties in the measured $L_{\rm x,(2-10)}$, no combination of P and $\dot{P}$ of the type $P^a \dot{P}^b$ can fit the data in a statistically acceptable way. However, it is remarkable that, among all the possible combinations of P and $\dot{P}$, the one which better describes the data selects again a scaling with $L_{\rm sd}$.

We note that all the data of Figure 4 lie under the critical line

$$L_{\rm x,crit} = 10^{-18.5} \left(\frac{L_{\rm sd}}{\rm erg\ s^{-1}} \right)^{1.48} \rm erg\ s^{-1} \qquad (6)$$

obtained searching for that line having the minimum *weighted* distance to the observed points. This line gives

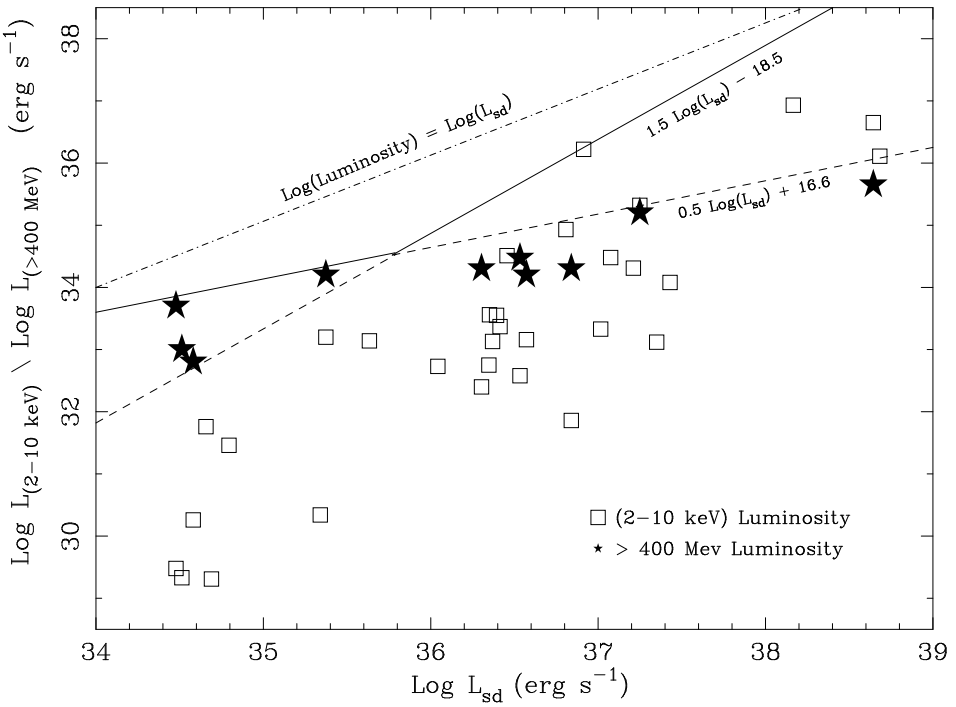

Fig. 5. High energy luminosity as a function of $L_{\rm sd}$ in two selected energy domains: in the (2-10) keV ($L_{(2-10){\rm keV}}$) and above 400 MeV ($L_{(>400{\rm MeV})}$). *Stars* represent young γ-ray pulsars taken from Zhang & Harding (2000; Fig. 3); *open squares* refer to the pulsars of our sample (with the exclusion of MSPs). The *dot-dashed line* gives the locus where luminosity equals the spin-down power. The *dashed lines* gives the critical luminosities (described as single power laws) in the two energy domains while the broken *solid line* interpolates the two lines, and indicates the observed change in slope, as discussed in section 5.

the maximum efficiency of conversion of spin-down energy in X-rays:

$$\eta_{\rm x} \equiv \frac{L_{\rm x,crit}}{L_{\rm sd}} = 10^{-18.5}\left(\frac{L_{\rm sd}}{\rm erg\ s^{-1}}\right)^{0.48}. \quad (7)$$

For $L_{\rm sd}$ in the interval $10^{32}-10^{38}$erg s^{-1}, the efficiency varies within $10^{-3} < \eta_{\rm x} < 0.8$.

5. Discussion

$L_{\rm x,crit}$ can be interpreted as the line giving the maximum luminosity that can be attributed exclusively to magnetospheric processes, and the large scatter below that line as due to additional mechanisms that tend to reduce $L_{\rm x}$ and that are independent of P and $\dot{P}$. Note that the width of the spread in the values of $L_{\rm x}$ does not vary over the whole interval of $L_{\rm sd}$, thus supporting further this interpretation.

The magnetospheric emission is pulsed and intrinsically anisotropic. Thus, the detection of a pulsed signal is susceptible to various geometrical corrections. In the computation of $L_{\rm x}$ we have assumed that the entire beam is seen. The angle α between the spin axis and the dipolar magnetic field controls the intrinsic width of the emission cone. According to Zhang & Harding (2000), $L_{\rm x}$ does depend on α. This effect is particularly pronounced for α=90^o and causes a drop in the luminosity. Disappointingly, it is still difficult to have a direct measure of α, which is known, with large uncertainty, only for a handful of sources (Miller & Hamilton 1993). The Vela pulsar is recognized to be an orthogonal rotator: this can explain the drop of $L_{\rm x}$ by $\sim 1-2$ orders of magnitude relative to $L_{\rm x,crit}$, making the observation consistent with the prediction, within the error determination. However, the small $\alpha \sim 30^o$ of PSR 0656+14 is not sufficient to explain its displacement from $L_{\rm x,crit}$. It is thus plausible that α influences the values of $L_{\rm x}$ but is not sufficient to explain the scatter seen in the $L_{\rm x}$ versus $L_{\rm sd}$ correlation.

Environmental effects can also be a source of scatter for the young pulsars of the sample. As an example, PSR 0537−69 is one order of magnitude less luminous than the Crab pulsar despite the similarity in the value of $L_{\rm sd}$ and in the apparent morphology. Wang et al (2001) explain the smaller efficiency in terms of a stronger confinement of the pulsar nebula by a surrounding star formation region, which combined with the high pulsar velocity (600 km s^{-1}) gives a smaller shock radius of a fraction of a parsec. The relativistic particles responsible for the X-ray emission thus escape the nebula in a time much shorter than the time of radiative energy loss.

The 2-10 keV energy band in which the sources are detected is selected by instrumental needs, but it is not necessarily optimal to sample the bulk of the broad-band high energy X-ray emission from pulsars. This is what emerges from a spectral analysis of a number of bright pulsars carried out with BeppoSAX data (Massaro et al. 2000). These new observations indicate that the photon spectral index (α) of the non-thermal emission is itself a function of energy $\alpha(E) = a + 2b\log(E/E_0)$ (with a and b parameters of the spectral fit and $E_0 = 1$ keV) that is consistent with the observational data when extrapolated in the UV-optical-IR range and at gamma-ray energies below 30 MeV. The spectral photon distribution peaks at a characteristic energy $E_{\rm max} = E_0 \cdot 10^{-a/4b}$ th from source to source. For Crab, $E_{\rm max} \sim 21$ keV so that the 2-10 keV interval contains a large fraction of $L_{\rm x}$. For Vela, the maximum would fall at about one MeV and then it would

imply a low $L_{\rm x}$, just as observed (relative to $L_{\rm x,crit}$). The existence of a characteristic energy or, more generally, of an energy threshold could cause the deviation of $L_{\rm x}$ from $L_{\rm x,crit}$.

The γ-ray luminosity (above 400 MeV) seems to follow a relation of the type $L_\gamma \propto L_{\rm sd}^{0.5}$ (Thompson et al. 1997; Thompson 2001). In Figure 5 we have drawn (in analogy to $L_{\rm x,crit}$ in the 2-10 keV band) the critical γ-ray luminosity (assuming emission in one steradian) $L_{\gamma,\rm crit} \sim 10^{16.6}(L_{\rm sd}/{\rm erg\ s^{-1}})^{0.5}{\rm erg\ s^{-1}}$ derived from Figure 5 of Zhang & Harding (2000). We note that at least three young pulsars (MSPs are excluded in this discussion), with high $L_{\rm sd}$ lie in between $L_{\rm x,crit}$ and $L_{\gamma,\rm crit}$. This indicates that for these sources the X-ray luminosity (in the interval 2-10 keV) dominates over L_γ, and that the correlation with $L_{\rm sd}$ of the luminosity integrated above 1 eV is steeper than indicated by Thompson (2001) above a value of $L_{\rm sd}$ which is around $10^{36} - 10^{36.5}{\rm erg\ s^{-1}}$ (as indicated in Figure 5). A possible interpretation of this steepening is that the physical mechanisms at play favor the emission in the X-ray channel when $L_{\rm sd}$ exceeds some value: cascade processes can develop fully so that higher generation pairs can produce photons at energies of only a few keV. In this framework one expects that the slope n of the efficiency which is a function of $L_{\rm sd}$ and of the selected energy band $\eta_{\bar\nu} \propto L_{\rm sd}^{n(\bar\nu)}$, (where $\bar\nu$ is the centroid frequency of the observational band) gradually increases when moving toward less energetic frequencies $\bar\nu$. Since the observed efficiency in the γ-ray energy band (above 400 MeV) is $\eta_\gamma \propto L_{\rm sd}^{-0.5}$ while in the 2-10 keV range varies as $\eta_{\rm x} \propto L_{\rm sd}^{0.5}$, we predict that the maximum efficiency should become almost independent of $L_{\rm sd}$ (i.e., $n \sim 0$) in an energy band intermediate the two. Future observations of pulsars in the energy range of *INTEGRAL* between (0.1-10) MeV may help in testing this prediction.

6. Conclusions

The analysis of the current data (with their uncertainties) on the non-thermal X-ray emission from rotation-powered pulsars shows:

1. No monomial combination of P and $\dot P$ fits $L_{\rm x,(2-10)}$ in a statistically acceptable way.
2. Still, a correlation between the X-ray luminosity in the band $2-10$ keV and $L_{\rm sd}$ persists in the data and the preferred scaling is $L_{\rm x,(2-10)} \propto P^{-4.00}\dot P^{1.34} \sim L_{\rm sd}^{1.34}$.
3. All the data lie below a critical line $L_{\rm x,crit} \propto L_{\rm sd}^{1.5}$, providing the maximum efficiency of conversion of $L_{\rm sd}$ in X-ray emission.
4. Geometrical effects, cut-off energy scales and environment could be the causes of the reduction in the detected $L_{\rm x,(2-10)}$, thus explaining the large scatter present in the data.

After comparing our results with those derived similarly in the γ-ray band, we suggest that the maximum efficiency of conversion of spin-down power in high energy emission should be almost independent of $L_{\rm sd}$ in the energy band that will be explored by *INTEGRAL*.

Acknowledgements. Part of this work was supported by the Italian ASI ARS 1R272000 grant. We thank the referee Yoshitaka Saito for very useful and stimulating comments.

References

Becker W., Trumper J., Lommen A.N., Backer D.C., 2000, ApJ, 545, 1015
Becker W., Trumper J., 1999, A&A, 341, 803
Becker W., Trumper J., 1997, A&A, 326, 682
Bildsten L. et al., 1997, ApJS, 113, 367
Camilo F., Kaspi V.M., Lyne A.G., et al., 2000, ApJ, 541, 367
Camilo F., Manchester R.N., Gaensler B.M., Lorimer D.R., Sarkissian J., 2002, ApJ, 567, L71
Chang H.K., Ho C., 1999, ApJ, 510, 404
Chang H.K., Ho C., 1997, ApJ, 479, L125
Cheng K.S., Gil J., Zhang L., 1998, ApJ, 493, L35
Cheng K.S., Zhang L., 1999, ApJ, 515, 337
Chevalier R.A., 2000, ApJ, 539, L45
Crawford F., Gaensler B.M., Kaspy V.M., et al., 2001, ApJ, 554, 152
Finley J.P., Srinivasan R., Saito Y., et al., 1998, ApJ, 493, 884
Finley J.P., Srinivasan R., Park S., 1996, ApJ, 466, 938
Finley J.P., Ogelman H., 1994, ApJ, 434, L25
Gotthelf E.V., Kaspi V.M., 1998, ApJ, 497, L29
Gotthelf E.V., Vasisht G., Boylan-Kolchin M., Torii K., 2000, ApJ, 542, L37
Greiveldinger C., Camerini U., Fry W., et al., 1996, ApJ, 465, L35
Grindlay J.E., Heinke C., Edmonds P.D., Murray S.S., 2001, Science, 292, 2290
Grindlay J.E., Camilo F., Heinke C., Edmonds P.D., Cohn, H., Lugger, P. 2002, ApJ, submitted, see also astro-ph/0112484
Halpern J.P., Camilo F., Gotthelf E.V., et al., 2001, ApJ, 552, L125
Halpern J.P., Wang F. Y-H., 1997, ApJ, 477, 905
Harrus I.M., Hughes J.P., Helfand D.J., 1996, ApJ, 464, L161
Hughes J.P., et al, 2001, ApJ, 559, L153
Kaaret P., Marshall H.L., Aldcroft T.L., et al., 2001, ApJ, 546, 1159
Kawai N., Tamura K., Saito Y., 1998, Advances in Space Research, 21, 213K
Kaspi V.M, Gotthelf E., Gaensler B.M, Lyutikov M., 2001, ApJ, 562, L163
Manchester R.N., 2001, PASA, 18, astro-ph/0009405
Marsden D., Blanco P.R., Gruber D.E., et al., 1997, ApJ, 491, L39
Marshall F.E., Gotthelf E.V., Zhang W., Middleditch J., Wang Q.D., 1998, ApJ, 499, L179
Massaro E., Cusumano G., Litterio M., Mineo T., 2000, A&A, 361, 695
Miller M.C., Hamilton R.J., 1993, ApJ, 411, 289
Mereghetti S., 2002, in *The Neutron Star Black Hole Connection*, ed. C.Kouveliotou, J.van Paradijs & J.Ventura, NATO ASI Ser. Dordrecht Kluwer, p.351, astro-ph/9911252
Mereghetti S., Bandiera R., Bocchino F., Israel G.L., 2002, ApJ, submitted
Mineo T., Cusumano G., Kuiper L., et al., 2000, A&A, 355, 1053

Murray S.S, Slane P.O., Seward F.D., Ramson S.M., Gaensler B.M., 2002, ApJ, in press, see also astro-ph/0108489
Nicastro L., et al, 2002, in preparation
Ögelman H., 1995, ASP Conference Series 72, ed. Fruchter A.S., Tavani M., Backer D.C., 309
Pavlov G.G., Zavlin V.E., Sanwal D., Burwitz V., Garmire G.P., 2001, ApJ, 552, L129
Pivovaroff M.J., Kaspi V.M., Camilo F., Gaensler B.M., Crawford F., 2001, ApJ, 554, 161
Pivovaroff M.J., Kaspi V.M., Gotthelf E.V., 2000, ApJ, 528, 436
Roberts M.S.E., Romani R.W., Johnston S., 2001, ApJ, 561, L187
Sakurai I., et al., 2001, PASJ, 53, 535
Saito Y., 1998, PhD thesis, Univ. of Tokyo (S98)
Saito Y., Kawai N., Kamae T., Shibata, S. Dotani T., Kulkarni S.R., 1997, ApJ, 477, L37
Seward F.D., Wang Z., 1988, ApJ, 332, 199
Slane P., 1994, ApJ, 437, 458
Slane P., Lloyd N., 1995, ApJ, 452, 115
Sun X., Aschenbach B., Becker W., et al, 1995, IAUC 6187
Takahashi M., Shibata S., Torii K., et al, 2001, ApJ, 554, 316
Taylor J.H., Cordes J.M., 1993, ApJ, 411, 674
Thompson D.J., Harding A.K., Hermsen W., Ulmer M.P., 1997, in *Proc. Fourth Compton Symposium*, ed. C.D. Dermer, M. S. Strickman, & J.D. Kurfess, AIP Conf. Proc. 410, 39 [TH97]
Thompson D.J., 2001, astro-ph/0101039
Torii K., Kinugasa K., Toneri T., et al, 1998, ApJ, 494, L207
Torii K., Saito Y., Nagase F., et al, 2001, ApJ, 551, L151
Torii K., Tsunemi H., Dotani T., et al, 1999, ApJ, 523, L69
Wang Q.D., Gotthelf E.V., Chu Y.-H., Dickel J.R., 2001, ApJ, 559,275
Wang F.Y-H., Halpern J.P., 1997, ApJ, 482, L159
Wang F.Y-H., et al, 1998, ApJ, 498, 373
Willingale R., Aschenbach B., Griffiths R.G., et al., 2001, A&A, 365, L212
Zhang B., Harding A.K., 2000, ApJ, 532, 1150